Journal of Materials Chemistry A

ROYAL SOCIETY OF CHEMISTRY

PAPER

View Article Online
View Journal | View Issue

Cite this: J. Mater. Chem. A, 2025, 13, 29415

Investigating the impact of alcohols on the morphology and structure of dendritic fibrous nanosilica (DFNS)†

Jawed Qaderi, [ab] Maryam Radjabian, *[a] Martin Held, [a] Anke-Lisa Höhme, [a] Erik Schneider, [a] Joachim Koll, [a] Sandra König, [c] Andreas Meyer, [b] Michael Fröba [c] and Volker Abetz *[ab]

Received 30th April 2025
Accepted 24th July 2025

DOI: 10.1039/d5ta03442f

rsc.li/materials-a

Dendritic Fibrous Nanosilica (DFNS) holds great promise for applications in various biomedical fields, CO_2 capture and conversion, catalysis, environmental remediation (or water treatment), and sensor development. While the impact of primary (linear) alcohols as co-surfactants in their synthesis has been investigated, the role of other alcohols beyond linear remains unexplored to date. In this study, we investigated the impact of different alcohols as co-surfactants on the morphology, structure, and physical properties of DFNS. We employed various primary, secondary, and tertiary alcohols, as well as diols with differing chain lengths and isomers. Significant variations in the specific surface area (S_{BET}) and total pore volume (V_p) were revealed across the samples, accompanied by notable morphological differences observed by scanning and transmission electron microscopy and small angle X-ray scattering. The highest S_{BET} and V_p values were found in samples synthesized with primary or linear alcohols, while much lower values were observed for samples synthesized with branched alcohols and diols. These findings emphasize the role of alcohols in governing the final morphology and structure of DFNS.

1. Introduction

Dendritic fibrous nanosilica (DFNS)[1–5] has recently attracted considerable interest in contemporary industries due to their unique properties and fibrous morphology. They possessed a spherical shape with fibers radiating outwards from the center of the spheres, resembling a sea urchin.[1,6,7] DFNS features promising physical properties, including high surface area, large pore volume, and good thermal and mechanical stability.[1,5,8–10] High surface area silica materials, including DFNS, have been successfully used in CO_2 capture,[11] CO_2 methanation,[12,13] catalysis,[14] photocatalysis,[11,15] solar cells,[16] heavy metal detection and removal,[17,18] drug delivery,[19] and other biomedical applications.[8]

Compared to other conventional mesoporous silica, such as the Mobil Composition of Matter No. 41 (MCM-41) family and Santa Barbara Amorphous-15 (SBA-15), DFNS stands out due to its unique three-dimensional fibrous structure, which enhances accessibility to active sites and improves performance in various applications.[20] This dendrimeric morphology, characterized by center-radial nanochannels and hierarchical nanopores, facilitates the passage of reactant molecules and efficient loading of guest species. The fibrous architecture arises from a microemulsion formed by surfactants, where the balance of hydrophobic and hydrophilic interactions among surfactants, precursors, hydrolyzing agents, and solvents governs the final structure.

In 2010, Polshettiwar *et al.* first developed fibrous silica nanospheres using tetraethyl orthosilicate (TEOS) as a silica source through a microemulsion system under microwave (MW)-assisted hydrothermal conditions, allowing them to create the unique dendritic fibrous structure characteristic of DFNS.[1] The inherent properties of DFNS can be finely tuned by adjusting various parameters. Bayal *et al.*[8] reported a facile protocol for synthesizing DFNS with different particle sizes, fiber densities, surface areas, and pore volumes by modifying reaction parameters including concentrations of urea, used as the base catalyst, cetyltrimethylammonium bromide (CTAB), a cationic surfactant used as the pore template or structure-directing agent, and 1-pentanol, used as the co-surfactant, as well as the reaction time, temperature, solvent ratio, and stirring time. They adjusted the particle size of DFNS from 170 nm to 1120 nm and controlled the fiber density from low to very

[a]Institute of Membrane Research, Helmholtz-Zentrum Hereon, Max-Planck-Str. 1, Geesthacht 21502, Germany. E-mail: maryam.radjabian@hereon.de; Tel: +49-4152-87-2802

[b]Institute of Physical Chemistry, University of Hamburg, Grindelallee 117, 20146 Hamburg, Germany. E-mail: volker.abetz@uni-hamburg.de; Tel: +49-40-42838-3460

[c]Institute of Inorganic and Applied Chemistry, University of Hamburg, Martin-Luther-King-Platz 6, Hamburg 20146, Germany

† Electronic supplementary information (ESI) available. See DOI: https://doi.org/10.1039/d5ta03442f

high, consequently tuning the pore volume from 0.23 $cm^3 g^{-1}$ to 2.18 $cm^3 g^{-1}$ with 1-pentanol. Additionally, they achieved a remarkable increase in the surface area of DFNS nanospheres, ranging from 315 $m^2 g^{-1}$ to 1244 $m^2 g^{-1}$ by varying the concentrations of urea and CTAB, reaction duration and temperature. In addition to this, several synthesis mechanisms have been proposed to address the formation of DFNS by taking into account the influence of different reaction conditions on the morphology and pore structure of the nanospheres. According to Maity *et al.*,[4] alcohols stabilize lamellar structures that eventually form DFNS by acting as co-surfactants in the bicontinuous microemulsion mechanism. Bahadur *et al.*[21] further conducted small-angle X-ray scattering (SAXS) investigations and established that the DFNS structure originates from direct modulation of the bicontinuous structure controlled by a surfactant, a co-surfactant, and the silicate species formed during hydrolysis and the condensation reaction of the silica precursor. Moon *et al.*[6] investigated the effect of oil/water ratios and found that the mesopore formation is controlled by the hydrolysis of TEOS at the oil–water interface, resulting in wrinkle-like structures.

Furthermore, by modifying the DFNS synthesis route, Li *et al.*[22] produced bioactive glass-based DFNS, highlighting how precursor selection affects the final morphology. Shen *et al.*[23] developed a biphasic stratification synthesis approach by emphasizing solvent-driven self-assembly, which allowed for precise control over hierarchical pore structures. It is also worth noting that Kalantari *et al.*[24] produced dendritic mesoporous organosilica nanoparticles (DMONs), highlighting how structural characteristics are affected by organic modifications. Du *et al.*[25] proposed a gas-diffusion-driven process, wherein the evaporation of a volatile solvent, *i.e.*, ethyl ether resulted in the formation of mesoporous silica and influenced radial pore structures. Moreover, Xu *et al.*[26] showed that the pore size and particle morphology of the monodispersed mesoporous silica nanoparticles are affected by solvent penetration, proposing a packing parameter model. Despite the fact that previous studies employed complex multi-step processes, the microwave-assisted hydrothermal synthesis approach offers a more rapid, simple, and economical method for producing fibrous silica nanoparticles with tuneable size and hierarchical porosity in a single step.

Prior studies have reported that silica morphology is significantly affected by the type and molar concentration of alcohols used as the co-surfactant. For example, Ahmad *et al.*[27] found that a higher alcohol content reduces the rate of TEOS hydrolysis, favoring particle growth over nucleation and producing larger particles. Particle morphology and size distribution are also affected by the amount of alcohol present. According to Niu *et al.*,[28] the absence of alcohol produces amorphous, irregular particles with a wider range of size distributions. Mirzaei *et al.*[29] found that by increasing the concentration of alcohol, the spherical mesoporous structures decreased. Wang *et al.*[30] tailored the fiber density and pore structure of mesoporous dendritic fibrous nanosilica by thoroughly changing the amount of *n*-amyl alcohol from 0.75 mL to 1.75 mL. Similarly, Bayal *et al.*[8] showed that tuning the volume of 1-pentanol could control the fiber density, surface area, pore volume, and particle size (about 170–1120 nm). Maity *et al.*[3] isolated the structural impacts of several types of primary alcohols on DFNS synthesis by maintaining fixed molar ratios. This approach allows more reliable attribution of morphological trends to alcohol characteristics.

Furthermore, studies on core–shell and mesoporous materials demonstrated that reagent ratios, including the surfactant and alcohol concentrations, can significantly alter nanoparticle nucleation and growth dynamics.[31,32] Alcohol structure, such as polarity, chain length, and branching, surely affects hydrolysis–condensation rates and interfacial interactions,[33] but, unless well regulated, its effects can be mixed with concentration-dependent variables.

The broader literature emphasizes the importance of alcohol structure in emulsion behavior during the hydrothermal synthesis process of DFNS nanospheres.[3,6,34–38] Emulsion stability largely depends on the molecular structure of the co-surfactant, especially the alkyl chain. In addition to the molecular structure, the molar ratio of alcohol to other reagents plays a key role in affecting the final morphology.[8,30] Prior studies[3,38] have solely covered the effects of primary alcohols with alkyl chain lengths ranging from three to six carbons. This leaves a gap in exploring the effects of different alcohols beyond primary alcohols as co-surfactants on the morphology and physicochemical properties of DFNS nanospheres. This study examines the impact of various alcohols—primary, secondary, tertiary, and diols with chain lengths of three to six carbons—on the synthesis of DFNS, focusing on their effects on nanoparticle shape, fiber density, and physical properties. The findings support the development of DFNS-based materials under controlled synthesis conditions. Several characterization techniques, such as scanning electron microscopy (SEM), transmission electron microscopy (TEM), dynamic light scattering (DLS), N_2 physisorption, small-angle X-ray scattering (SAXS), and thermogravimetric analysis (TGA), were employed to broadly investigate the properties of the synthesized DFNS samples.

2. Results and discussion

2.1 Morphological and structural characteristics

We investigated the effect of different types of alcohols on the dendritic morphology, structure, and physical properties of DFNS nanospheres. For this purpose, different primary, secondary, tertiary alcohols, and diols with varying chain lengths and isomers were selected. The corresponding alcohol names and molecular formulas, alcohol/TEOS molar ratios, and abbreviations of the samples are given in Table 1.

In this study, a fixed volume (0.5 mL) of alcohol was used in each synthesis to ensure consistency within the small-scale constraints of the 20 mL vessel. As a result, the alcohol/TEOS molar ratios varied between samples (see Table 1), depending on the molecular weight of the alcohol. The CTAB/TEOS molar ratio was kept constant at 0.23 to ensure comparable micelle templating conditions. Notably, 0.5 mL of each alcohol was

Table 1 List of alcohols used for DFNS samples along with their corresponding molecular structures, alcohol/TEOS molar ratios, and sample abbreviations

Alcohol name	Molecular structure	Alcohol/TEOS molar ratio	Sample abbreviation
1-Propanol		1.67	D1P
1-Butanol	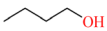	1.36	D1B
1-Pentanol	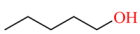	1.15	D1Pe
1-Hexanol	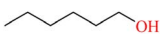	0.99	D1H
2-Propanol		1.63	D2P
2-Butanol		1.36	D2B
2-Pentanol		1.15	D2Pe
2-Hexanol	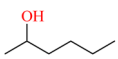	0.99	D2H
3-Pentanol		1.15	D3Pe
3-Hexanol	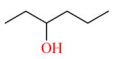	1.00	D3H
t-Butanol		1.31	D*t*B
2-Methyl-2-butanol		1.14	D2M2B
2-Methyl-2-pentanol		1.02	D2M2Pe
1,2-Butanediol	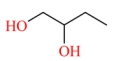	1.38	D12BD
1,2-Pentanediol	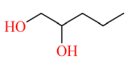	1.16	D12PeD
1,2-Hexanediol	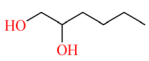	1.00	D12HD

sufficient to yield well-defined DFNS nanospheres following hydrothermal synthesis.

The unique bicontinuous morphology of DFNS is often described using various terms, reflecting interpretations based on either SEM or TEM observations. The SEM (Fig. 1) and TEM (Fig. 2) images show well-defined spherical shaped particles with dendritic morphology, confirming their successful synthesis through a microemulsion system using the MW-assisted hydrothermal technique. Interestingly, all DFNS produced with different types of alcohols show unique bicontinuous concentric lamellar morphologies, as previously reported for primary alcohols.[13,20,39–41] These particles inherently possess a fibrous structure, characterized by fibres extending radially from the core to the shell. The fibre density in the core region was notably higher than in the shell, as observed in the TEM images of all DFNS samples (Fig. 2). The type of alcohol utilized as a co-surfactant had a significant impact on the fibrous structure. Alcohols such as 1-butanol, 1-pentanol, 1-hexanol, 2-hexanol, and 3-hexanol formed uniform particles with open fibrous structures in D1B, D1Pe, D1H, D2H, and D3H, respectively (Fig. 1b–d, h and j and $2b_1$–d_1, h_1 and j_1). Moderately fibrous particles were formed in the case of D1P, D2B, D2Pe, D3Pe, D*t*B, D2M2Pe, and D12HD when 1-propanol, 2-butanol, 2-pentanol, 3-pentanol, *t*-butanol, 2-methyl-2-pentanol, and 1,2-hexanediol were employed as co-surfactants, respectively (Fig. 1a, f, g, i, k, m and p and $2a_1$, f_1, g_1, i_1, k_1, m_1 and p_1). Moreover, compact and dense particles were formed for D2P, D2M2B, D12BD, and D12PeD, when using 2-propanol, 2-methyl-2-butanol, 1,2-butanediol, and 1,2-pentanediol, respectively (Fig. 1e, l, n and o and $2e_1$, l_1, n_1 and o_1). We observed that a higher number of carbon atoms, particularly in the backbone of the alcohol, can promote the formation of more porous structures, even in the case of branched alcohols and diols as seen in D3H and D12HD. The synthesis of DFNS is influenced by the complex interactions between alcohol head groups, surfactants, and silicic acid, which determine the emulsion stability pattern. These interactions ultimately affect the particle shape, final structure, and morphology of the nanospheres. In this approach, CTAB,[20] a well-known surfactant used in nanoparticle formation, has a positively charged,

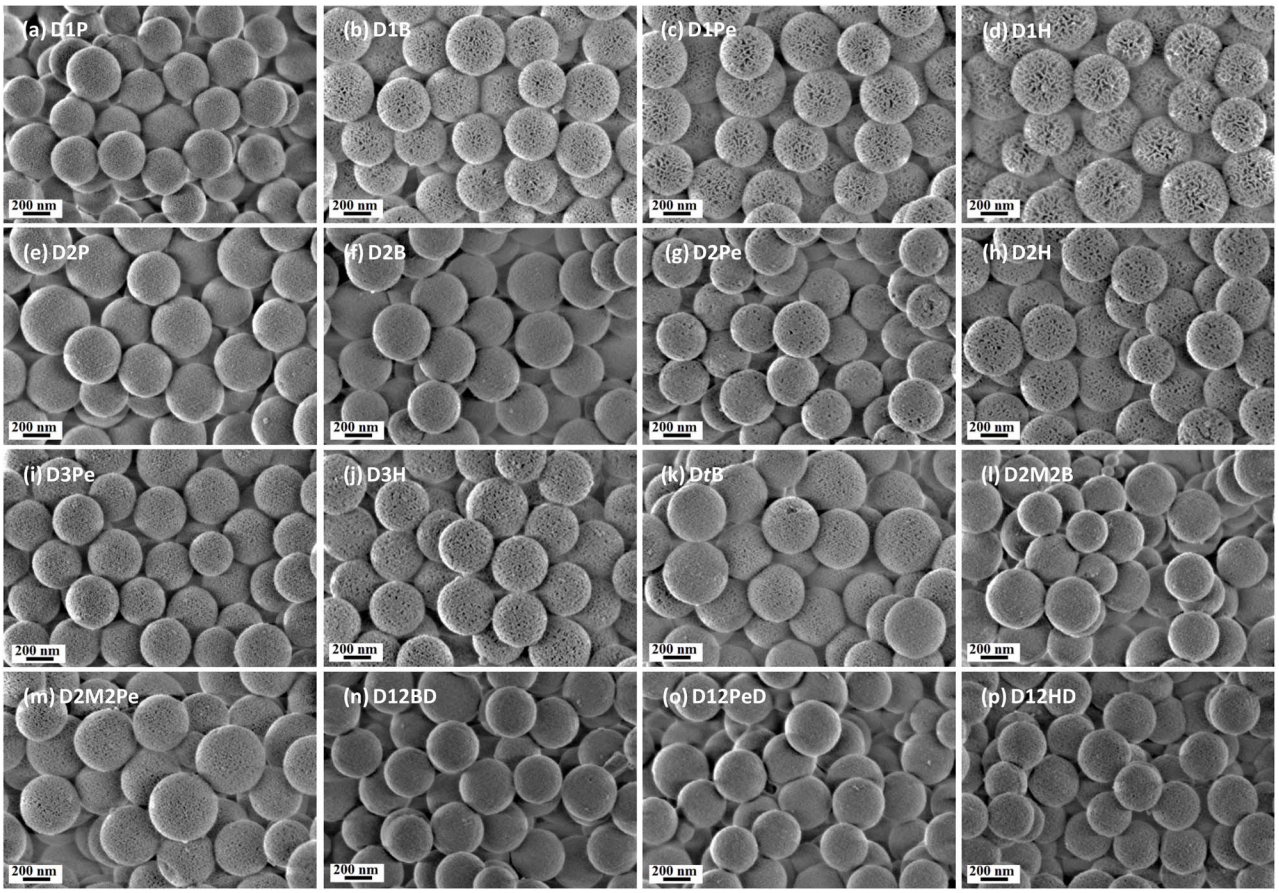

Fig. 1 SEM images of the synthesized DFNS using different alcohols: primary alcohols in (a) D1P, (b) D1B, (c) D1Pe, and (d) D1H; secondary alcohols in (e) D2P, (f) D2B, (g) D2Pe, (h) D2H, (i) D3Pe, and (j) D3H; tertiary alcohols in (k) D*t*B, (l) D2M2B, and (m) D2M2Pe; diols in (n) D12BD, (o) D12PeD, and (p) D12HD.

hydrophilic head group and plays a multifaceted role in stabilizing micelles or emulsion droplets while exerting control over the growth dynamics of silica nanospheres.

Based on studies on emulsion stability,[3,34] the increase in stability was due to an increase in the structural similarity between CTAB and the alcohol carbon chain. An increase in the hydrophobic–hydrophobic interactions and a reduction in the headgroup–headgroup repulsion of the CTAB quaternary ammonium by the insertion of the neutral, polar alcoholic headgroup increased the stability of emulsions.[3]

The hydrolysis of TEOS in the presence of urea produces silicic acid, which also interacts with head groups of surfactants and water molecules to promote the formation of stable emulsions. Moreover, it takes part in condensation and hydrolysis reactions. The dual functionality of silicic acid enhances both the hydrophilic character of microemulsion droplets and the structural integrity of the resulting nanospheres.

The linear structures of alcohols with intermediate to long carbon chains, such as unbranched primary alcohols 1-butanol, 1-pentanol, and 1-hexanol in D1B, D1Pe, and D1H, respectively, as well as the longer-chain secondary alcohols, 2-hexanol and 3-hexanol in D2H and D3H, facilitated efficient packing at the cyclohexane–water interface. This promotes strong hydrophobic–hydrophobic interactions and reduces interfacial tension to enhance emulsion stability, which led to the formation of uniform particles with open fibrous structures (Fig. 1b–d, h and j and $2b_1$–d_1, h_1 and j_1).

In addition, 1-propanol, with a shorter linear carbon chain in D1P (Fig. 1a and $2a_1$), and branched alcohols with intermediate carbon chain lengths such as 2-butanol, 2-pentanol, 3-pentanol, and *t*-butanol in D2B, D2Pe, D3Pe, and D*t*B (Fig. 1f, g, i and k and $2f_1$, g_1, i_1 and k_1), led to the formation of moderately fibrous structures with a less open morphology. Similarly, 2-methyl-2-pentanol and 1,2-hexanediol with longer carbon chains in D2M2Pe and D12HD (Fig. 1m and p and $2m_1$ and p_1), respectively, also produced less open morphologies. In both the former and latter cases, the higher number of carbons in these alcohols—rather than their bulkiness or location of the hydroxyl group—was the dominant factor for the stability of the emulsion in these systems, resulting in more effective nucleation and growth processes during the formation of these nanospheres.

On the other hand, 2-propanol, with a short, branched carbon chain in D2P (Fig. 1e and $2e_1$), and 2-methyl-2-butanol, a more highly branched and substituted tertiary alcohol in D2M2B (Fig. 1l and $2l_1$), introduced greater branching and

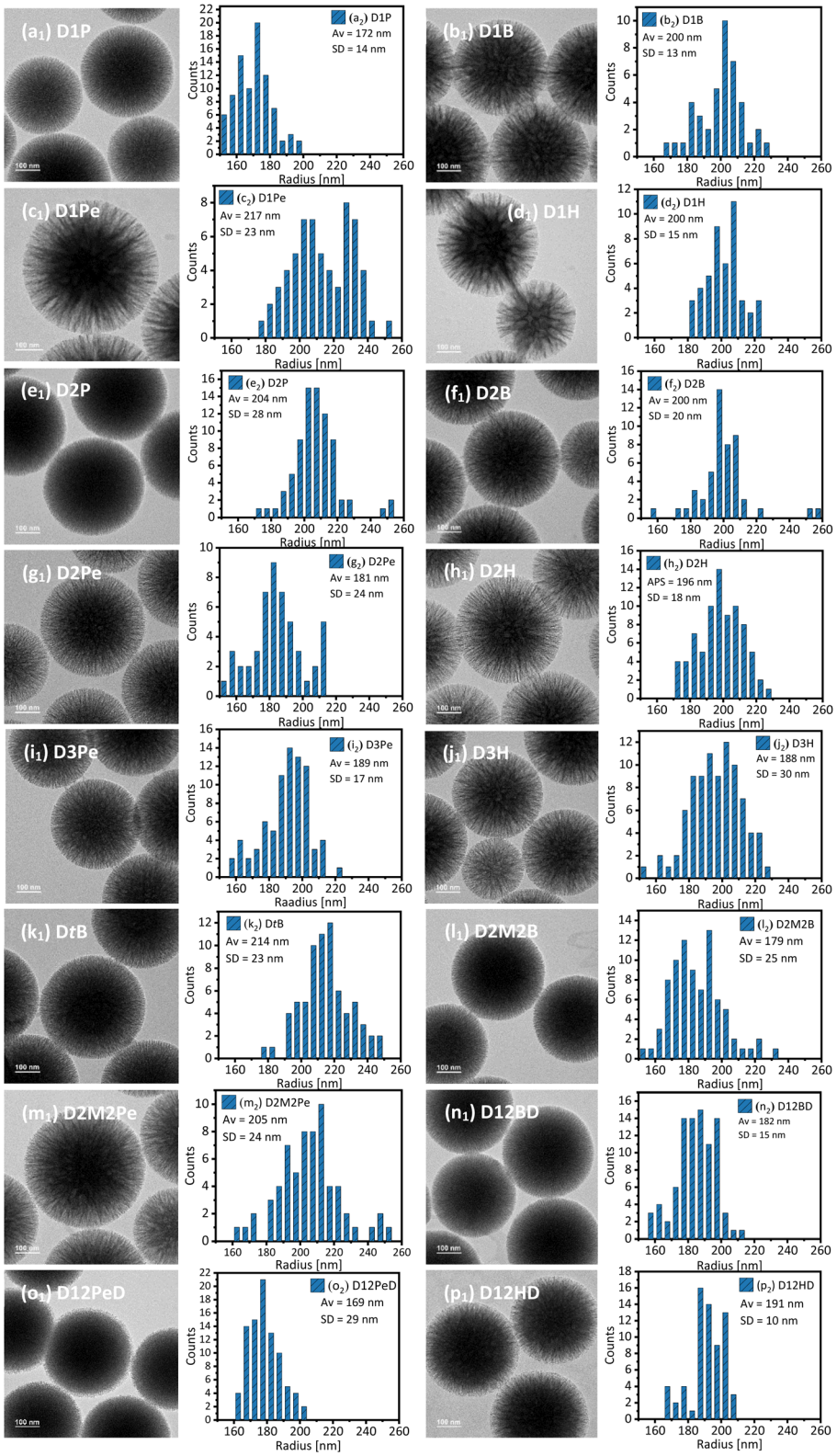

Fig. 2 TEM images and particle size distributions of the synthesized DFNS using different alcohols: primary alcohols in (a_1 and a_2) D1P, (b_1 and b_2) D1B, (c_1 and c_2) D1Pe, and (d_1 and d_2) D1H; secondary alcohols in (e_1 and e_2) D2P, (f_1 and f_2) D2B, (g_1 and g_2) D2Pe, (h_1 and h_2) D2H, (i_1 and i_2) D3Pe, and (j_1 and j_2) D3H; tertiary alcohols in (k_1 and k_2) D*t*B, (l_1 and l_2) D2M2B, and (m_1 and m_2) D2M2Pe; diols in (n_1 and n_2) D12BD, (o_1 and o_2) D12PeD, and (p_1 and p_2) D12HD.

additional alkyl groups along the carbon chain. Due to the steric hindrance caused by this branching, alcohol molecules are unable to pack efficiently at the interface, resulting in weakened hydrophobic–hydrophobic interactions and a smaller reduction in interfacial tension, both of which decrease the emulsion stability. The instability of these emulsions led to the formation of dense particles with compact fibrous structures, reflecting the influence of alcohol branching on emulsion stability and particle characteristics.

Our findings on the influence of branched and substituted alcohols on emulsion stability and DFNS formation align well with the results of Thampi *et al.*,[42] who explored the effects of alcohol structure on microemulsion stability. Their study demonstrated that the molecular geometry of branched alcohols influences interfacial behavior, highlighting the role of co-surfactants in modulating emulsion properties.

Similarly, the addition of diols such as 1,2-butanediol and 1,2-pentanediol in D12BD and D12PeD (Fig. 1n and o and $2n_1$ and o_1), respectively, decreased the emulsion stability and further influenced the interactions between silicic acid and the head group of CTAB, leading to the formation of compact and dense particles. These diols, with an additional hydroxyl group, exhibit hydrophilic characteristics, while their alkyl chains provide hydrophobic properties. Due to the complex structure of diols, the arrangement of surfactant molecules may also impact the hydrophobic core of micelles or emulsion droplets.

Variations in the alcohol/TEOS molar ratios have less impact on DFNS morphology than the type and molecular structure of alcohol, as shown in Fig. 2. For example, 1-pentanol, 2-pentanol, 3-pentanol, 2-methyl-2-butanol, and 1,2-pentanediol all have comparable alcohol/TEOS molar ratios (~1.15–1.16), but the resulting particles exhibit different morphologies, ranging from open fibrous (D1Pe) to moderately fibrous (D2Pe and D3Pe), and even to compact and dense in the case of D2M2B and D12PeD. Similar patterns were observed for alcohols with six carbon atoms. Even though the alcohol/TEOS molar ratios were almost the same, 1-hexanol and 2-hexanol created open fibrous morphologies, 3-hexanol produced moderately fibrous particles, and 2-methyl-2-pentanol and 1,2-hexanediol produced relatively denser structures. Similarly, although both 1-propanol and 2-propanol prepared with high molar ratios, 1.67 and 1.63, respectively, the former produced moderately fibrous DFNS, while the latter led to compact structures. These illustrations support the finding that DFNS morphology is primarily shaped by the alcohol's structure, including its linearity, branching, and hydroxyl group position, with the molar ratio playing a secondary and less significant role.

This study underscores the pivotal role of the molecular structure of co-surfactants in determining the emulsion stability and nanoparticle architecture, focusing on their impact rather than addressing the well-established formation mechanism of DFNS.

The particle size distributions from the TEM imaging are presented in Fig. $2a_2$–p_2. The mean particle size fell within the range of 170 to 220 nm. Fig. 3 shows the relationship between the average TEM-measured radius of DFNS samples along with their corresponding standard deviation, based on the type of

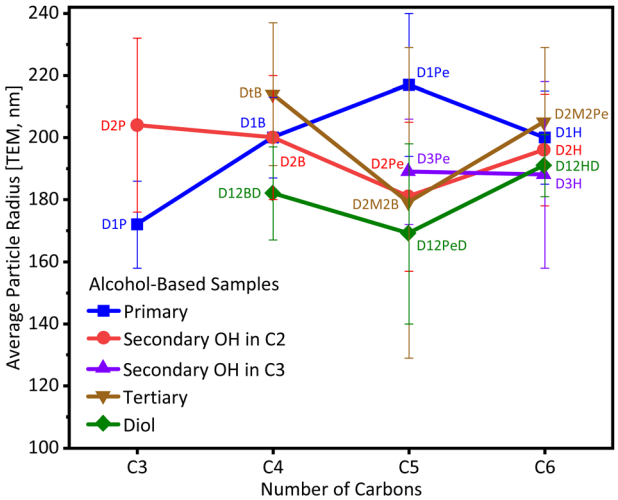

Fig. 3 The relationship between the TEM-measured radius of DFNS samples and the type of alcohols used in their synthesis.

alcohol used in their synthesis. Among primary alcohols, D1P forms the smallest particles, followed by an increase in size in D1B and D1Pe, then a decrease in D1H, whereas the alcohol/TEOS molar ratio decreased across these samples. In contrast, for samples with secondary alcohols, a slight reduction in particle size is observed, with the largest average radius for D2P and the smallest for D2Pe. The DFNS samples with diols such as 1,2-hexanediol and 1,2-butanediol exhibited smaller particle sizes, with average particle radii of 191 nm and 182 nm, respectively, compared to their analogous primary and secondary alcohol counterparts. Furthermore, samples with comparable carbon content—D1Pe, D2Pe, D3Pe, D2M2B, and D12PeD sharing a similar alcohol/TEOS molar ratio (~1.15)—showed a decreasing size trend from linear to branched to diol structures. This emphasizes that alcohol geometry and functional group configuration—rather than the molar ratio—govern the final DFNS particle size.

In addition, DLS was employed to determine the number-weighted hydrodynamic radius distribution of DFNS, as summarized in Fig. 1S.† DLS analysis revealed bimodal, and in some samples, trimodal radius distributions, with the main peak located in the range of approximately 150 to 220 nm. The presence of an additional peak below 100 nm (*e.g.*, in D2B and D3Pe) in DLS results may arise from very small particles, broken particles or even noise. In some DFNS samples, such as D12PeD, D12BD and D1B, DLS revealed a bimodal distribution, with a secondary peak above 200 nm, showing a comparable intensity to the dominant primary peak. This observation is partially consistent with the particle size distribution seen in TEM images, keeping in mind that the hydrodynamic radii exceed the TEM-observed radii in principle. However, the difference in measurement conditions and volume of analysis will contribute to a divergence in particle radius distributions between TEM and DLS.

Possibly, in DLS, a more fibrous morphology increases the effective hydrodynamic radius due to the extended solvation

shell that traps solvent molecules.[43,44] Moreover, the peak observed above 250–300 nm may arise from loosely associated agglomerates of the dispersed particles. The high density of silanol groups on the silica surface is expected to promote the formation of multiple hydrogen bonds among the particles. The higher silanol density and surface energy strengthen interparticle interactions, which reduce the dispersion stability. As a result, the nanospheres in some samples may form temporary agglomerates rather than remaining well-dispersed as primary particles.[45] Physical entanglement between particles,[46,47] which may promote the formation of larger, intertwined structures, is another explanation for the peak seen in the DLS findings above 200 nm. Agglomerates in the dry state of TEM imaging were observed but disregarded for high magnification. These can be explained by capillary forces that might cause strong attractive forces to overcome repulsive interactions during the last stages of drying, which leads to the formation of larger aggregates.[48,49] The same effects will play a role in the dry-state application of DFNS nanospheres in CO_2 adsorption. Generally, DLS and TEM show reasonable agreement in the observed size ranges of the dominant peak. Thus, the trends observed in both methods consistently reflect the influence of alcohols as co-surfactants on the particle radius and radius distribution of DFNS.

Remarkably, in our work, no noticeable decrease in particle size was observed when varying the alcohol chain length—from 1-propanol to 1-butanol, 1-pentanol, and 1-hexanol—or when using their secondary and tertiary isomers, such as 2-propanol, 2-butanol, 2-pentanol, 2-hexanol, 3-pentanol, 3-hexanol, *t*-butanol, 2-methyl-2-butanol, and 2-methyl-2-pentanol, or their diol counterparts, including 1,2-butanediol, 1,2-pentanediol, and 1,2-hexanediol. This contrasts with the results of Maity *et al.*,[3] who found that switching the co-surfactant from 1-pentanol to 1-hexanol dramatically reduced the particle size from approximately 450 nm to 50 nm. In their case, the size of the particles (~50 nm) remained unchanged for all subsequent long-chain alcohols. They used a reaction temperature of 82 °C *via* conventional refluxing, whereas we employed a higher reaction temperature of 120 °C under microwave irradiation. This represents a significant difference between our work and theirs.

Maity *et al.*[3] attributed the significant reduction in particle size to the coalescence phenomenon, which plays a pivotal role in stabilizing DFNS formed from bicontinuous microemulsion droplets (BMDs). They ascribed the particle size reduction (from ~500 nm to ~50 nm) to the coalescence process. Their observation indicated that while 1-pentanol-BMDs underwent coalescence, 1-hexanol-BMDs remained stable and did not experience coalescence, due to their increased stability. However, the stability of the BMDs formed by longer chain alcohols, 1-hexanol, gradually increased. Maity *et al.* proposed that the abrupt size decrease was related to the energy required for coalescence. Specifically, a reaction temperature of 82 °C was sufficient for the coalescence of 1-pentanol-BMDs, resulting in larger DFNS particles, whereas the more stable 1-hexanol-BMDs did not coalesce at this temperature. They synthesized DFNS using 1-hexanol-BMDs at different temperatures (76, 82, 86, and 90 °C) and observed an increase in particle size from about 50 nm to 110 nm as the reaction temperature increased, providing additional evidence in support of their hypothesis. Notably, even with extended reaction times, the particle size stayed mostly unchanged at a fixed temperature, suggesting that temperature is essential for BMD coalescence. In contrast, our use of a higher reaction temperature of 120 °C for a reaction time of four hours under microwave conditions provided enough energy to form stable BMDs, which acted as the nanoreactor or template for nucleation and growth steps, leading to the formation of DFNS. This suggests that coalescence is likely occurring in our system, contributing to the formation of larger DFNS. Moreover, the accelerated nucleation and growth rates induced by microwave irradiation may have further enhanced the size of the final product. The results underscore the key role of reaction temperature and energy input in controlling the final particle size and morphology of DFNS. Changes in the co-surfactant structure directly affect the formation and growth of nanospheres and potentially alter the properties and applications of the resulting materials.

2.2 Study of textural properties

The textural properties of the synthesized DFNS samples were thoroughly analyzed using N_2 physisorption analysis conducted at 77 K, as depicted in Fig. 4, which illustrates the N_2 adsorption–desorption isotherms for all samples. Following the IUPAC classification,[50–52] all DFNS samples exhibited a type-IV isotherm pattern accompanied by an H3-type hysteresis loop.[53,54] Despite the minor variations in loop size observed in the hysteresis loops (Fig. 4a–p), all DFNS samples exhibited a similar type of loop. These differences are attributed to variations in pore size distribution (Fig. 2S and 3S ESI†) and in fiber densities (Fig. 1a–p and $2a_1$–p_1).

However, there exists controversy regarding the type of hysteresis loop for DFNS. While Fatah *et al.*,[37] Yusof *et al.*,[55] and Hamid *et al.*[56] considered DFNS to have an H1-type hysteresis loop, Palanichamy *et al.*[53] and Febriyanti *et al.*[20] classified it as an H3-type hysteresis loop. According to IUPAC regulations, an H1-type loop is often associated with porous materials consisting of agglomerates, resulting in narrow pore size distributions. The former studies also reported DFNS particles having a narrow range of uniform mesopores with a well-defined cylindrical-like pore channel. Conversely, according to the IUPAC classification, an H3-type loop is observed in aggregates of plate-like particles, leading to slit-shaped pores, as confirmed by later studies. These findings suggest that DFNS nanospheres exhibited the typical H3 hysteresis loop, characteristic of solids with slit-shaped pores.[57]

The formation of this type of isotherm is indicative of multilayer adsorption followed by capillary condensation,[51,52] offering a clear indication of mesopores within the material. The TEM micrographs (Fig. $2a_1$–p_1) revealed the fibrous structure of silica nanospheres, with V-shaped mesopores arising from the spatial gaps between silica fibers within individual particles. The V-shaped mesopores observed in TEM images are consistent with the slit-shaped pore geometry suggested by the H3-type hysteresis loop in the N_2 physisorption data. These

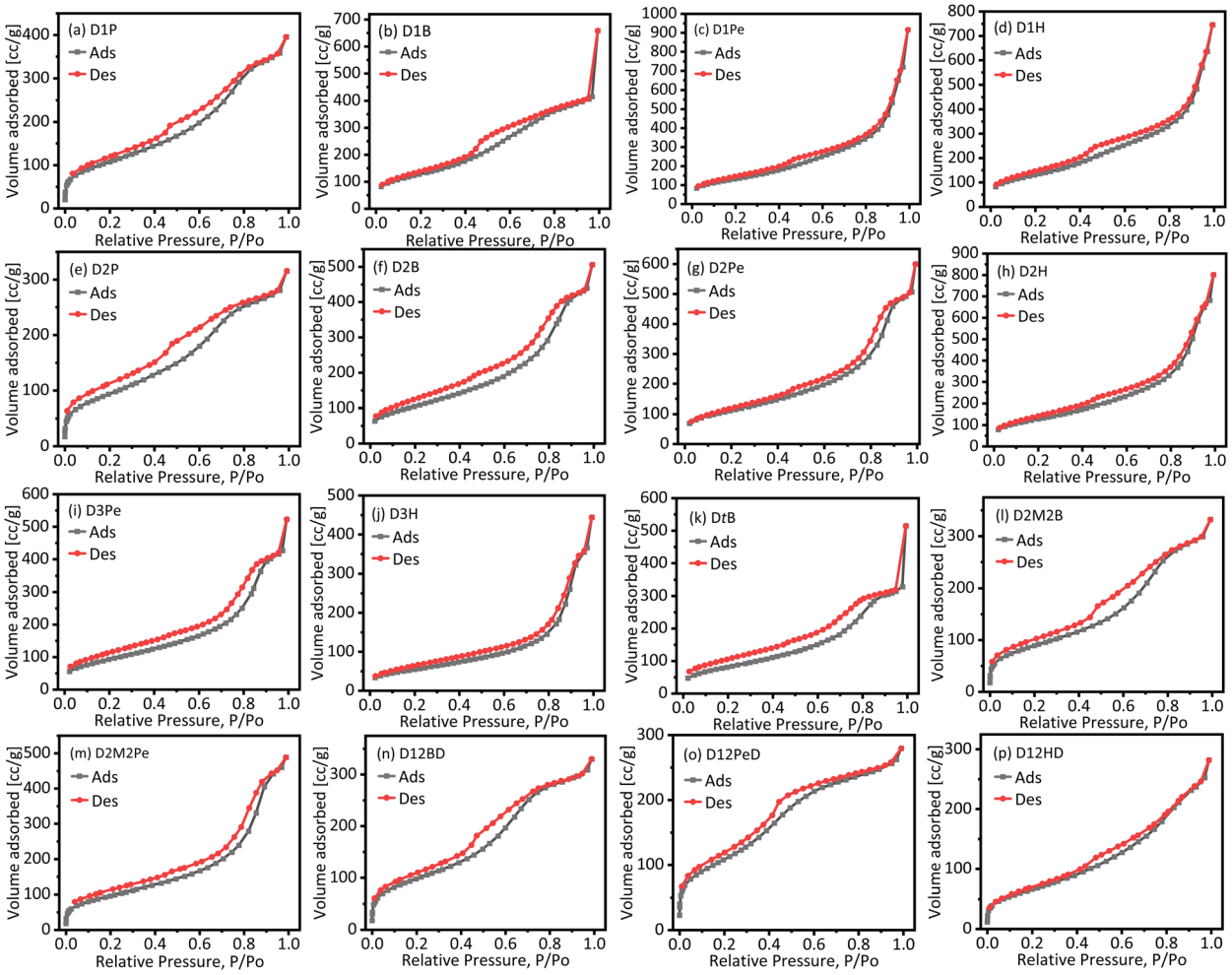

Fig. 4 N_2 physisorption isotherms of synthesized DFNS using different alcohols: primary alcohols in (a) D1P, (b) D1B, (c) D1Pe, and (d) D1H; secondary alcohols in (e) D2P, (f) D2B, (g) D2Pe, (h) D2H, (i) D3Pe, and (j) D3H; tertiary alcohols in (k) D*t*B, (l) D2M2B, and (m) D2M2Pe; diols in (n) D12BD, (o) D12PeD, and (p) D12HD. Ads refers to Adsorption and Des to desorption.

results highlight the relationship between the fiber arrangement observed in microscopy and the textural properties deduced from adsorption analysis. This unique pore structure is characteristic of DFNS particles and distinguishes itself from the tubular or cylindrical type of MCM-41/SBA-15 porous materials.[58,59]

The specific surface area (S_{BET}) determined by the Brunauer–Emmett–Teller[60] method, and the total pore volume (V_p) and average pore diameter (d_p) values obtained from the desorption branch of the Barrett–Joyner–Halenda (BJH) plots, are summarized in Table 2. Spheres with less dense or open fibrous structures exhibit higher surface area and pore volume, while denser spheres have lower surface area and pore volume. These results are in good agreement with those obtained by Bayal *et al.*[8] The DFNS samples synthesized with various alcohols revealed noticeable behaviors in S_{BET} and V_p, highlighting the complex relationship between the molecular structure of the alcohol and the properties of the synthesized materials. Although the alcohol/TEOS molar ratio is also known to influence micelle organization and silica condensation, our experimental results suggest that it is not the primary factor affecting the S_{BET} and V_p of DFNS materials.

As shown in Fig. 5a and b, the specific surface area and total pore volume generally increase from D1P to D1Pe, where the alcohol/TEOS molar ratio decreased from 1.67 to 1.15 (Table 1). This trend indicates that longer-chain alcohols facilitate the formation of larger micelles during synthesis, which in turn promotes the formation of a more porous silica structure, larger pores and an increased surface area. However, a slight decrease in pore volume is observed for D1H (Fig. 5b), which may be attributed to differences in the packing efficiency of the surfactant–alcohol interactions, leading to variations in pore formation.

The S_{BET} and V_p values are generally slightly lower in secondary alcohols compared to primary alcohols of identical chain length. For instance, D2P exhibited slightly lower S_{BET} and V_p values compared to D1P. This trend persisted as observed in D2B to D2Pe to D2H. This indicated that even changing the position of the hydroxyl group in the alcohol chain has a significant impact on the surface area and pore volume of

Table 2 Summary of textural properties of all DFNS samples prepared using different co-surfactants

Sample	S_{BET}[a] [m^2 g^{-1}]	V_p[b] [cm^3 g^{-1}]	d_p[c] [nm]	N_2 uptake [cm^3 g^{-1}]
D1P	396	0.53	3.68	396
D1B	464	0.96	3.69	658
D1Pe	474	1.34	3.67	916
D1H	477	1.06	3.51	745
D2P	348	0.40	3.74	315
D2B	387	0.70	3.64	506
D2Pe	402	0.87	3.66	600
D2H	465	1.16	3.69	801
D3Pe	347	0.73	3.64	523
D3H	202	0.65	3.85	444
D*t*B	302	0.72	3.67	515
D2M2B	321	0.46	3.76	332
D2M2Pe	350	0.68	3.69	488
D12BD	357	0.45	3.65	330
D12PeD	403	0.23	3.44	279
D12HD	245	0.40	3.70	282

[a] Surface area of samples measured by the BET method from the adsorption branch of the N_2 physisorption process. [b] Total pore volume calculated using the BJH method. [c] Pore diameter obtained from BJH.

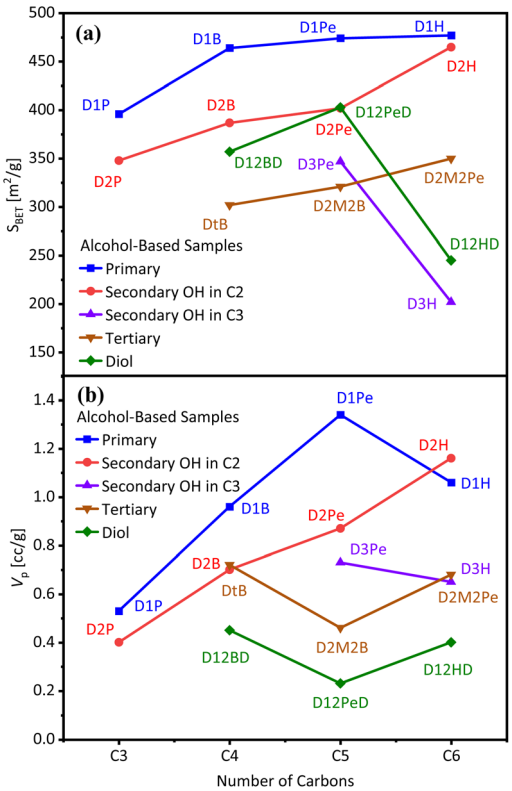

Fig. 5 Relationship between the (a) S_{BET} and (b) V_p of DFNS samples with the number of carbons in different type of alcohols as co-surfactants.

the relevant DFNS species. This was further confirmed by using 3-pentanol and 3-hexanol. D3Pe and D3H, exhibited an even further decrease in both S_{BET} and V_p. The drastic reduction in values observed for D3H may be attributed to the compromised surfactant packing efficiency and hindered micelle formation, potentially caused by specific steric constraints introduced by branching in the 3-hexanol structure.

The complex balance between the chain length, branching and isomeric effects in alcohols was further investigated. The introduction of structural branching or isomerism led to a reduction in both S_{BET} and V_p values compared to their linear counterparts. For example, D*t*B exhibited a dramatic decrease in surface area and pore volume, whereas in D1B and even D2B this was not observed. Moreover, incorporating tertiary alcohols such as 2-methyl-2-butanol and 2-methyl-2-pentanol into the analysis provided further insights into the impact of branching on material properties. For instance, D2M2B and D2M2Pe showed a decrease in both the surface area and total pore volume as compared to D1Pe, D2Pe, D1H, and D2H. These findings highlighted the effect of steric hindrance in tertiary alcohols, which affected the surfactant self-assembly by reducing the emulsion and micelle stability, resulting in moderately fibrous or less open particle formation with smaller and closed pores and channels.

Finally, the introduction of diols, including 1,2-butanediol, and 1,2-pentanediol, expanded the understanding of how dual hydroxyl groups and their spatial arrangement impact material properties. D12BD and D12PeD displayed S_{BET} and V_p values lower than their monohydroxy counterparts, suggesting that the presence of multiple hydroxyl groups may not significantly enhance the surface area or pore volume in this context. The decrease in emulsion and micelle stability due to enhanced hydrophilic–hydrophilic interactions among the CTAB head group, silicic acid, and hydroxyl groups of the alcohols[34,35] resulted in the formation of compact and dense particles with smaller surface areas and total pore volumes compared to those with monohydroxy alcohols, as also reported by Bayal *et al.*[8]

As observed in the linear primary alcohol series (C3–C6), a decrease in the alcohol/TEOS molar ratio in some secondary alcohol-derived samples from D2P (1.63) to D2B (1.36), D2Pe (1.15) and D2H (0.99) leads to higher S_{BET} and V_p (Table 2), indicating improved surfactant packing and micelle formation at lower alcohol concentrations.[8] It is supported by prior studies showing that decreasing the co-surfactant content can enhance micelle organization and thus promote mesostructure formation.[27,30]

Interestingly, within the samples prepared with alcohols of identical carbon chain lengths and nearly comparable alcohol/TEOS ratios (Table 1), such as D1Pe, D2Pe, D3Pe, D2M2B, and D12PeD, the S_{BET} and V_p values are markedly affected by variations in molecular structure complexity. The surface characteristics vary widely: D1Pe shows the highest S_{BET} and V_p (Table 2), while D12PeD shows significantly lower values. In the samples prepared with the hexanol series, despite having similar alcohol/TEOS molar ratios, the samples D1H, D2H, D3H, D2M2Pe, and D12HD show significant deviations as well. D1H and D2H exhibit high S_{BET} and V_p, while D3H, D2M2Pe, and D12HD show a marked decline in porosity. Furthermore, despite the similar reagent ratios in D2M2B and D12PeD, the branching and additional hydroxyl groups appear to hinder

micellar assembly and limit silica condensation, resulting in denser structures. These findings demonstrate that, although the molar ratio affects textural characteristics, the type and structure of the alcohol used as a co-surfactant are the primary determinants of DFNS surface area and pore development.

The N_2 uptake values of all the synthesized samples at the relative pressure of $P/P_O = 0.4–0.9$ are also given in Table 2. It was noted that linear alcohols with longer carbon chain lengths including 1-pentanol, 1-hexanol, and 1-butanol facilitated the higher N_2 uptake values of 916, 745, and 658 $cm^3\ g^{-1}$, respectively, in their corresponding DFNS samples, *i.e.*, D1Pe (Fig. 4c), D1H (Fig. 4d), and D1B (Fig. 4b), respectively. However, 1-propanol resulted in a very low N_2 uptake value of 396 $cm^3\ g^{-1}$ in D1P (Fig. 4a). The same patterns were observed for DFNS samples synthesized using the secondary alcohols of the same carbon chain length, such as 2-propanol, 2-butanol, 2-pentanol, 2-hexanol, 3-pentanol, and 3-hexanol. The order of N_2 uptake was D2H > D2Pe > D3Pe > D2B > D3H > D2P, all of which showed lower uptake than their counterparts prepared with primary alcohols.

The N_2 uptake was further decreased in the case of samples synthesized using tertiary alcohols, such as *t*-butanol, 2-methyl-2-butanol, and 2-methyl-2-pentanol, with the order of N_2 uptake being D2B > D2M2Pe > D2M2B, which again exhibited lower uptake than their counterparts produced using primary (linear) and secondary (branched) alcohols. The main reason for these findings is the reduced S_{BET} and V_p values in these DFNS samples, caused by the steric hindrance from the branched and bulky structures of secondary, and especially tertiary alcohols. This hindrance weakens the hydrophobic–hydrophobic interactions, resulting in inefficient surfactant packing and micelle formation. Consequently, the micelle and microemulsion become less stable during the nucleation and growth of nanospheres. These observations were further confirmed by introducing diols, such as 1,2-butanediol, 1,2-pentanediol, and 1,2-hexanediol, during the synthesis of DFNS. Samples like D12BD and D12PeD exhibited the lowest N_2 uptake values of 330 $cm^3\ g^{-1}$ (Fig. 4n) and 279 (Fig. 4o), respectively. The introduction of two hydroxy groups likely reduced the hydrophobic interactions due to the increased hydrophilic interactions among the hydrolyzed silicic acid, alcohol head group, and the quaternary ammonium of CTAB, as mentioned earlier, which led to decreased micelle or emulsion stability, resulting in more compact and denser nanospheres with lower S_{BET} and V_p values. Despite this, D2H with 2-hexanol stands out in the second rank after D1Pe with 1-pentanol among all the samples. This result indicates that the longer the alcohol carbon chain the less the steric hindrance to some extent which helps stabilize the corresponding microemulsion system and leads to less dense nanospheres with open morphology.

The pore size distribution (distance between fibers or channel size) of all synthesized DFNS samples measured using both the adsorption and desorption branches of the BJH method[61] is given in Fig. 2S and 3S (ESI),† respectively. The pore size distribution exhibits a distinct feature, spanning a wide range of length scales, in contrast to MCM-41 and SBA-15 materials, which show only a narrow mesopore size distribution. The graphs in Fig. 3S (ESI)† show a narrow unimodal pore size distribution for D1P, D1B, D1Pe, D1H, and D2P. In contrast, D2B, D2Pe, D2H, D3Pe, D3H, D*t*B, and D2M2Pe exhibited a bimodal distribution. The pore size distribution of these samples is followed by a broad peak in a higher size range, typically around 10–25 nm. Overall, the narrow peaks around 3–6 nm can be attributed to the size of micelles, and the broader peaks are related to the inter-dendrimer distance between dendrimers, thus confirming their mesoporous characteristics.[12,51]

The difference in the N_2 uptake and pore size distribution of each DFNS sample is due to their difference in inter-dendrimer distance. D1P, D2P, D12BD, D12PeD, and D12HD showed smaller inter-dendrimer distances, while inter-dendrimer distances in some parts of D2B, D*t*B, D2M2B, and D2M2Pe were probably too small to be considered pores, which could lead to the changes in their respective isotherms. The difference in inter-dendrimer distance also affected the total pore volume and surface area of each sample, as shown in Table 2.

2.3 Small-angle X-ray scattering (SAXS) of DFNS

We further investigated the structural properties of the synthesized materials using SAXS, a powerful technique for studying porous materials.[62,63] This technique provides detailed information on the internal structure, repeat distances, and wall or sheet thickness of nanospheres, which are influenced by the type of co-surfactant used during synthesis. The SAXS profiles of the calcined (550 °C and 6 h) DFNS samples with various alcohols are shown in Fig. 6a–d. Among the DFNS samples, D1B, D1Pe, and D1H (Fig. 6a), D2B, D2Pe, D2H, and D3H (Fig. 6b), as well as D*t*B, D2M2B, and D2M2Pe (Fig. 6c), exhibited a broad scattering feature in the SAXS profiles, indicating a lower degree of structural ordering within the

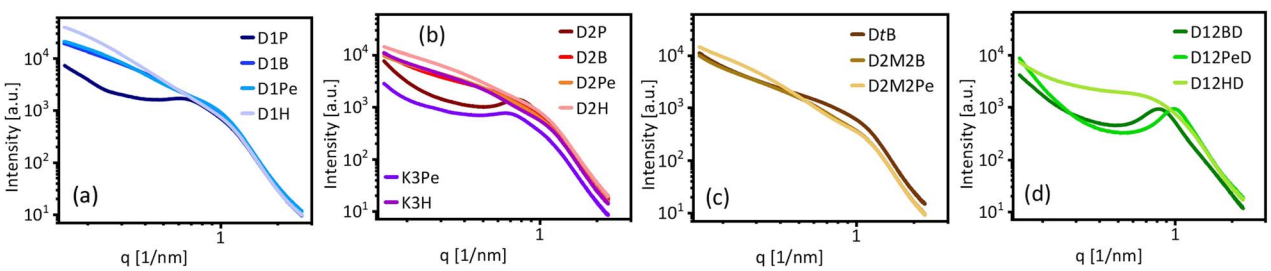

Fig. 6 SAXS profiles of synthesized DFNS samples prepared with (a) primary alcohols, (b) secondary alcohols, (c) tertiary alcohols, and (d) diols.

mesostructured nanospheres. Conversely, samples, including D1P, D2P, D3Pe, D12BD, D12PeD, and D12HD, exhibited increased reflection intensities in their SAXS profiles, indicating a more ordered mesostructure comparable to that of other well-known mesoporous materials like SBA-15 and MCM-41.[64] The presence of sharper reflections for these nanospheres indicates a higher degree of structural regularity, which can be attributed to their moderately fibrous structures or denser and more compact morphologies consistent with TEM images in Fig. 2.

A clear relationship between the type of co-surfactant and the resulting structural properties, more specifically, the repeat distance, is revealed by the SAXS investigation of DFNS. The repeat distance (d) can be determined from the scattering vector (q) at which the first peak in the SAXS pattern occurs, using Bragg's law $d = 2\pi/q$.[62] The wall thickness (t) of DFNS samples was determined using the density correlation function ($g1$) obtained from SAXS analysis. This approach provides insights into structural changes, such as possible sheet collapse, which may influence the measured wall thickness. The d and t of the DFNS nanospheres are clearly marked on the SEM image of D1Pe presented in Fig. 7, providing a visual representation of the structural parameters, and the values of these parameters are tabulated in Table 1S.† No systematic change in wall thickness was observed for all samples prepared with different alcohols, hence their effect is constricted to the repeat distance. However, when comparing the repeat distance to electron microscopy images, one should keep in mind that SAXS averages over the entire particle volume, while SEM and TEM reveal the repeat distance on the surface and the outer layer, respectively.

The type of co-surfactant affects the repeat distances of DFNS samples. Samples prepared using primary alcohols, including 1-butanol to 1-hexanol, exhibit repeat distances that decrease from 7.2 to 5.7 nm for D1B to D1H as the carbon chain length increases, while the alcohol/TEOS molar ratios decreases. Additionally, samples such as D2H and D3H, prepared using a similar alcohol/TEOS molar ratio along with longer carbon chain secondary alcohols of 2-hexanol and 3-hexanol, respectively, showed repeat distances of 6.3 and 6.0 nm. According to this trend, alcohols with longer carbon chains improve the stability of fibrous structures and produce a less open mesoporous framework.[3] Thus, the increased hydrophobicity associated with longer alkyl chains likely facilitated improved silica polymerization, promoting well-defined mesoporous fibrous structures. Samples prepared using secondary alcohols, including 2-propanol to 3-pentanol, exhibited repeat distances between 6.2 and 7.0 nm, resulting in moderately fibrous or less open structures compared to primary alcohols. The introduction of steric hindrance due to the secondary carbon configuration limits the expansion of the framework, leading to shorter repeat distances.

The most compact structures are produced by secondary alcohols possessing a shorter carbon chain, such as 2-propanol in D2P, and branched or tertiary alcohols, such as 2-methyl-2-butanol in D2M2B. These samples have repeat distances of 6.6 and 6.0 nm, respectively. These alcohols more restrict the polymerization of the silica species during the nucleation and growth steps, which results in the formation of dense mesostructures. These findings are consistent with the previous research that highlights the importance of steric effects in defining the structural properties of the mesoporous materials.[42]

Similarly, the DFNS samples synthesized with diols, such as D12BD and D12PeD, exhibited a decrease in repeat distance as the carbon length increased from C4 to C5 (6.8 to 5.7). The diols used to synthesize D12BD and D12PeD have additional hydroxyl groups, which increase the hydrophilic–hydrophilic interactions. The framework became compact because of these interactions. However, 1,2-hexanediol with a longer carbon chain led to the formation of a moderately open silica framework in D12HD (Fig. 1p and $2p_1$). This observation shows that the effect of carbon chain length is more dominant than the effect of the number of hydroxyl groups in DFNS synthesis.[65] According to this complex interaction, diols as co-surfactants can lead to a variety of mesostructures.

Across the sample set, identifying the relationship between the SAXS-derived repeat distances, alcohol/TEOS molar ratios, and alcohol structure is somewhat challenging. For the samples prepared with alcohols of identical carbon number, a higher molar ratio sometimes seems to correspond to slightly larger repeat distances; for instance, D1P (1.67) and D2P (1.63) have repeat distances of 7.0 and 6.6 nm, respectively. The difference between repeat distances may arise from the alcohol structure and alcohol/TEOS molar ratio. The former exhibits a moderately fibrous structure (Fig. $2a_1$) and the latter shows a compact and dense morphology (Fig. $2e_1$). Similarly, D2Pe, despite having a higher molar ratio of 1.15 shows a larger repeat distance than D2H (0.99). This pattern does not, however, apply to every sample. For example, for the samples prepared using primary alcohols, D1B (1.36) despite having a lower alcohol/TEOS molar ratio than D1P (1.67) exhibits a slightly larger repeat distance

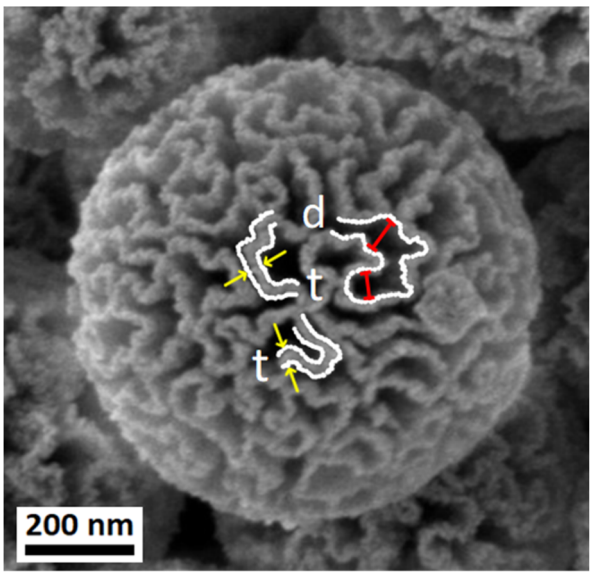

Fig. 7 SEM image of a DFNS nanosphere, with the annotated repeat distance (d) shown by the red lines and wall thickness (t) indicated by the distance between two yellow arrows, highlighting key structural parameters.

(Table 1S†) and an open fibrous morphology (Fig. 2b$_1$). Among the samples prepared using diols, D12BD (1.38) and D12PeD (1.16) show decreasing repeat distances (6.8 to 5.7 nm) despite only modest changes in the molar ratio, with both exhibiting compact and dense morphologies (Fig. 2n$_1$ and o$_1$). On the other hand, D12HD (1.00) exhibits a moderately fibrous structure (Fig. 2p$_1$) and a repeat distance of 6.9 nm, reversing the trend. These findings suggest that micelle organization and framework regularity appear to be primarily influenced by the molecular structure, including hydroxyl distribution and steric effects, rather than by alcohol concentration.

2.4 TGA studies

The TGA curves of the calcined DFNS samples (see Fig. 2S†) exhibit two distinct stages between 25 °C and 800 °C. Fig. 8 presents the total weight loss and the weight loss analysis of calcined DFNS samples prepared using different alcohols, measured under atmospheric air at 120 °C and 800 °C.

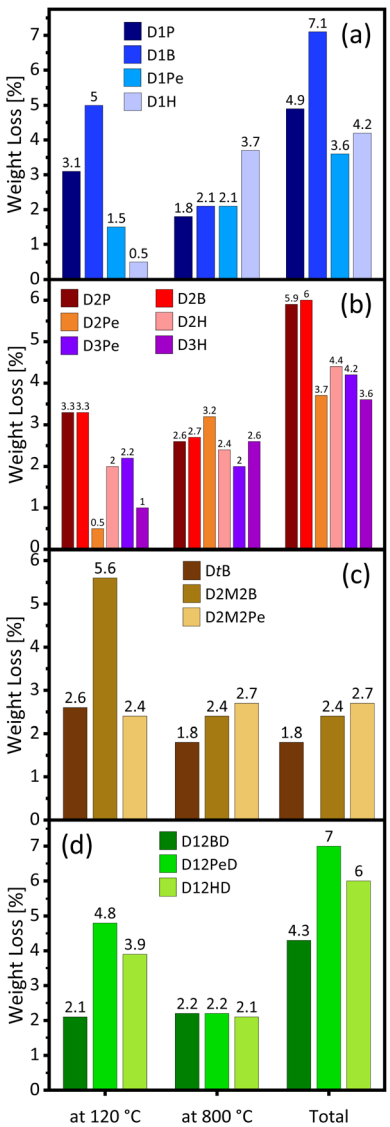

Fig. 8 Weight loss (%) of DFNS at 120 °C and 800 °C plotted for samples prepared with (a) primary alcohols, (b) secondary alcohols, (c) tertiary alcohols, and (d) diols.

The first stage, occurring between 25 °C and 120 °C, can be primarily attributed to the removal of physically and chemically adsorbed volatile species such as organic solvents used during the synthesis, as well as surface-adsorbed water.[1,66,67] The weight loss observed in the first stage showed slight deviations from the systematic pattern in samples prepared with primary alcohols compared to those prepared with secondary alcohols, tertiary alcohols, and diols. For instance, D1B showed a higher weight loss of 5% (Fig. 8a) compared to D2B with a weight loss of 3.3% (Fig. 8b). Similarly, D2M2B showed a higher weight loss of 5.6% (Fig. 8c) compared to D1H (0.5%) and D2M2Pe (2.4%) prepared with longer carbon-chain alcohols. This suggests that the lower the number of carbons, the higher the hydrophilicity of the corresponding DFNS sample, which adsorbs greater amounts of water, leading to increased weight loss in this range. This conclusion was further confirmed in the case of DFNS samples prepared with diols (Fig. 8d). For instance, D12PeD displayed a notable weight loss of 4.8% due to increased hydrophilicity from additional hydroxyl groups. This behavior aligns with literature reports linking the higher hydroxyl content and greater hydrophilicity to increased water adsorption and mass loss during initial heating stages.[68]

Although Fig. 8 indicates that DFNS produced with more hydrophilic alcohols often exhibits more weight loss in the 25–120 °C range, there are some alcohol pairs that clearly deviate from this pattern. The notable anomaly observed between D1P and D1B, where D1P shows lower weight loss despite 1-propanol being more hydrophilic than 1-butanol is due to its shorter carbon chain. Also, even though 2-pentanol should be more hydrophilic than 2-hexanol based on the shorter chain length alone, D2Pe shows less weight loss than D2H.

Although hydrophilicity plays a role in water adsorption and with the ensuing TGA weight loss, these variations indicate that it is not the only reason. Alcohol structure and DFNS characteristics seem to be related in a more intricate way than just hydrophilicity or chain length. The steric bulk structure of the alcohols, their interactions with CTAB micelles, and their effects on micelle packing and pore formation are some of the factors that may be causing variations in weight loss trends. Furthermore, alcohol volatility—defined by differences in evaporation rates—may influence the local concentrations of reactants during synthesis, particularly under microwave conditions, thereby affecting the condensation kinetics and final porosity. Together, these variables influence the amount of water retained in the structure and contribute to the explanation of the unusual weight loss trends seen in the TGA range of 25 to 120 °C.

The type of alcohol used had an important effect on the specific surface area, pore volume, and pore size distribution of DFNS samples; independent of surface hydrophilicity, larger pore volumes may be able to retain more water molecules. For example, despite being synthesized with less hydrophilic alcohols, D1B and D2H can retain more water because they have a higher specific surface area and a larger total pore volume or more mesopores than D1P and D2Pe, respectively (Table 2).

The alcohol/TEOS molar ratio also influences water retention behavior, although its impact appears secondary to the molecular structure of alcohols. Samples with higher alcohol/TEOS molar ratios, such as D1P (1.67) and D2P (1.63), show relatively higher first-stage weight losses (Fig. 8a), consistent with increased hydrophilicity and water adsorption. Similarly, the higher weight loss in D2M2B (Fig. 8c) correlates with its high molar ratio (1.36), supporting the expected trend. However, several inconsistencies reveal that molar ratio alone cannot explain the observed thermal behavior. For example, D1B (1.36) shows a significantly higher weight loss (Fig. 8a) than D1P (Fig. 8a), despite a lower alcohol/TEOS ratio. Even more striking, D1H (0.99) and D2Pe (1.15) both show minimal water loss (Fig. 8a and b, respectively), despite their lower molar ratios. Moreover, D2H, with a comparable molar ratio of 0.99, exhibits a much higher weight loss (Fig. 8b). These deviations suggest that molecular features such as branching, hydroxyl group position, and evaporation rate exert a stronger influence on water retention than the alcohol amount alone.

Another aspect causing the irregular weight loss trend in the 25–120 °C range is the presence of adsorbed co-surfactant molecules and loosely bound CTAB residues. While CTAB decomposition typically occurs at higher temperatures (above ~200 °C), small amounts of physically adsorbed or loosely retained CTAB can partially desorb at lower temperatures due to weak surface interactions. The extent of this retention varies slightly between samples because of micellar interactions based on the alcohol structure used during synthesis. Secondary and branching alcohols have an impact on micelle stability, which leads to different CTAB encapsulation efficiencies and consequent surface retention.[69] At temperatures between 25 and 120 °C, these residual molecules may desorb, resulting in mass losses that are not solely attributed to water adsorption.

The second weight loss step, observed between 120 and 800 °C, is mainly due to the thermal decomposition of silanol hydroxyl groups (Si–OH) and residual organic moieties (CTAB).[70] This step is indicative of the dehydroxylation process, called progressive condensation of silanols, which is supposed to take place above 190 °C, according to the observations and the reported literature.[71]

The weight loss in the second stage increased from samples prepared using primary alcohols to those prepared using secondary alcohols. The small weight loss in D1B, D1Pe and D3Pe suggests that longer-chain primary and secondary alcohols enhance the thermal stability of the corresponding silica samples. However, higher weight loss values observed in the case of D1H, D2H, and D3H prepared using 1-hexanol, 2-pentanol, and 3-hexanol, respectively, highlight the reduced stability of the particles. Furthermore, D2M2Pe displayed a loss value of 2.7%, attributed to the steric hindrance, and D12PeD displayed a weight loss of 2.2%, due to increased hydrophilicity from additional hydroxyl groups, which both destabilized the silica network.

In general, samples synthesized with higher alcohol/TEOS molar ratios, like D1P (1.67) and D2P (1.63), show somewhat higher second-stage weight losses. This is consistent with the hypothesis that a higher residual organic content results from increased alcohol availability. However, this trend does apply for all sample sets. For example, even though D1B (1.36) and D2B (1.36) have lower molar ratios than D1P and D2P, they exhibit greater weight losses. Similarly, while having lower alcohol contents, D2Pe (1.15) and D2H (0.99) both show comparatively significant second-stage losses (Fig. 8b). These inconsistencies indicate that micelle packing, porosity, and hydroxyl trapping within the silica network are more significantly modulated by alcohol structure than by concentration. Consequently, the alcohol/TEOS molar ratio is a relevant factor, but it cannot account for TGA trends alone—alcohol molecular design remains the dominant parameter.

Three main factors may contribute to these observations. First, the amount of CTAB incorporated during synthesis may vary based on the alcohol structure. The micelle packing and silica condensation rates are changed by secondary alcohols such as 2-propanol, 2-butanol, and 2-pentanol. This may increase CTAB entrapment in the silica matrix and result in increased weight loss during thermal decomposition. Second, different samples, especially those produced with secondary alcohols, may have varying amounts of residual organics due to variations in washing efficiency, which could lead to greater weight loss. However, this may not apply uniformly to all samples.

Third, surface silanol groups, particularly those remaining after sintering, especially within the pore walls or less-condensed regions, in DFNS synthesized with these secondary alcohols—may be distributed differently or have a higher density, which would result in greater weight loss during dehydroxylation. These structural and chemical variations are often determined by the molecular interactions between the alcohols and silica precursors which take place during the synthesis.

The TGA results emphasize that the thermal behavior, stability, and composition of DFNS are significantly influenced by the type, chain length, branching, and the number of hydroxyl groups of the alcohols used as the co-surfactant during the synthesis process.

3. Experimental

3.1 Chemicals

Tetraethyl orthosilicate (TEOS, ≥99%), cetyltrimethylammonium bromide (CTAB, ≥99%), 1-propanol (anhydrous, 99.9%), 2-propanol (99.95%), 1-butanol (99.9%), 2-butanol (99.5%), *t*-butanol (anhydrous, ≥99.5%), 2-pentanol (≥98%), 2-methyl-2-butanol (anhydrous, ≥99%), 3-pentanol (98%), 1-hexanol (99%), 2-hexanol (99%), 3-hexanol (98%), 2-methyl-2-pentanol (99%), 1,2-butanediol (≥98.0%), 1,2-pentanediol (96%), 1,2-hexanediol (97%), ethanol (96% and absolute) and acetone (HPLC grade) were purchased from Sigma-Aldrich (Germany). Cyclohexane (≥99.9%), urea (≥99%), and 1-pentanol (≥98.5%) were purchased from Merck Millipore (Germany). Demineralized water was used for all experiments. All the chemicals used were of analytical grade and were used without further purification.

3.2 Synthesis of DFNS

The synthesis of DFNS was conducted using the MW-assisted hydrothermal method, which was adopted from a study by

Polshettiwar and colleagues with some minor modifications.[1] In a typical synthesis, 0.835 g of TEOS was dissolved in a solution of 10 mL of cyclohexane and 0.5 mL of alcohol (co-surfactant), which was stirred at 700 rpm for 30 min and denoted as solution A. In the meantime, 0.334 g of CTAB and 0.2 g of urea were added to 10 mL of distilled water, which was stirred at 1200 rpm for 30 min, and it was marked as solution B. The solution B was added dropwise into solution A in 5 minutes, and the whole reaction mixture was stirred at 1200 rpm for 60 minutes at room temperature. The resultant microemulsion solution was placed in a Teflon-sealed microwave reactor, and the hydrothermal synthesis process was carried out under MW irradiation with a maximum power of 400 W at 120 °C for 4 hours, with constant stirring at 800 rpm and a maximum pressure of 7 bar inside the reaction vessel during the synthesis process. Various DFNS samples were prepared by changing the type of alcohol (Table 1). After the hydrothermal process, the microwave reactor was cooled to room temperature. Subsequently, the resulting DFNS was separated by centrifugation at 10 000 rpm for 10 min and then washed three times with absolute ethanol and then three times with distilled water. The freshly separated product was dried in an oven in air at 110 °C for 24 h. The product was calcined in a Linn High Therm GmbH tubular furnace with a 5 °C min^{-1} ramp to 550 °C, held for 6 hours in air to remove the surfactant or template, followed by controlled cooling to room temperature. After calcination, the powder was ground using a mortar. The MW-assisted hydrothermal synthesis was carried out using an Anton Paar microwave reactor: Monowave 450 (Austria).

3.3 Characterization methods

The morphology and structure of all the synthesized DFNS were examined using scanning electron microscopy (SEM) and transmission electron microscopy (TEM). SEM images were recorded on a Merlin (ZEISS, Oberkochen, Germany) microscope at an accelerating voltage of 1 kV and a probe current of 15–30 pA. Before microscopic analysis, particles were sputter-coated with 1.5 nm platinum using a CCU-010 coating device (Safematic, Switzerland). TEM images were recorded in bright field mode using a Tecnai™ G^2 F20 (FEI Thermo Fisher Scientific) microscope operating at an acceleration voltage of 200 kV, equipped with a Gatan OneView camera for high-resolution imaging. Before analysis, a 2 μL ethanol dispersion was drop-cast onto a carbon-coated copper grid, and the sample was dried in air. The particle size in TEM images was measured manually by drawing lines on the 4 k high-resolution images (.dm3 files) using Gatan's Digital Micrograph software. The samples were collected directly from the fresh reaction mixture after four hours of irradiation, without any additional treatments such as washing, centrifugation, drying, and calcination.

Dynamic light scattering (DLS) experiments were conducted using a particle size analyzer from ALV GmbH (Langen, Germany) with a 5004 correlator and an ALV/CGS-3 goniometer with a wavelength of about 532 nm to measure the hydrodynamic size of the nanospheres. The measurements were conducted at room temperature at 90°. For sample preparation, 2 mg of sample was dispersed in 2 mL of water, resulting in a 0.1% concentration. The dispersion was sonicated for 3 minutes at room temperature to ensure uniformity. Each sample was measured three times for 300 s. The density correlation functions ($g1$) were fitted to extract the number weighted distribution function with the ALV-correlator software V3.0.

The textural properties of the prepared DFNS samples were identified through N_2 physisorption assessments on a QuadraSorb SI MP (Quantachrome Instruments) surface area analyzer at −196 °C. Before the N_2 sorption analysis, the samples (∼100 mg) were degassed in an external degasser (MasterPrep Degasser, Quantachrome Instruments) at 120 °C for 20 hours under vacuum to ensure the complete removal of adsorbed gases and moisture. Isotherm, BET surface area, total pore volume and pore size distribution were analyzed using Quantachrome software QuadraWin, version 7.1.

The small-angle X-ray scattering (SAXS) measurements were conducted on a self-designed SAXS apparatus which was equipped with an Incoatec™ X-ray source IμS, Quazar Montel optics and scatterless pinholes, providing a focal spot size diameter of 700 μm at the sample and a wavelength of 0.1542 nm. An evacuated flight tube with a 1.1 m distance between the sample and detector was used, and a CCD-Detector Rayonix™ SX165 was employed for detection. The regular measurement time per sample was 10 minutes. SPEC (ver. 5.32) developed by Certified Scientific Software, Cambridge, MA, USA, was used as the control software. The data were analyzed using the correlation function option in SasView (ver. 5.0.6).

Thermal gravimetric analysis (TGA) was performed using a TG 209 F1 Iris®, Fa. Netzsch instrument. The analysis was performed in the temperature range of 25 to 800 °C with a temperature ramp-up of 5 °C min^{-1}.

4. Conclusion

In this study, we utilized different types of alcohols, including primary, secondary, tertiary alcohols, and diols, to tailor the morphology and structure of DFNS. We investigated the morphology, structure, and physicochemical properties of the materials using SEM, TEM, DLS, N_2 physisorption, SAXS, and TGA. All the synthesized materials showed spherical morphology with fibrous structures, with variations in fiber density from the core to the shell. Higher carbon content and linear alcohols promoted the formation of a more open and fibrous structure due to stronger hydrophobic–hydrophobic interactions, which stabilized the microemulsion system during synthesis. In contrast, branched alcohols and diols resulted in denser, more compact particles, as steric hindrance decreased hydrophobic interactions, while diols also enhanced hydrophilic interactions with CTAB's quaternary amine and hydrolyzed silicic acid from TEOS. The particle sizes remained stable across all samples. The high reaction temperature of 120 °C provided sufficient energy for the coalescence of stable bicontinuous microemulsion droplets (BMDs) and thus did not cause any significant size variation. These droplets acted as nanoreactors, facilitating the nucleation and growth of DFNS. The specific surface area (S_{BET}) of the materials ranged from 202 m^2

g^{-1} to 477 m^2 g^{-1}. The highest values were observed for DFNS synthesized with primary (linear) alcohols of longer chain length, while the lowest values were recorded for those synthesized using branched alcohols and diols. The total pore volume (V_p) of the particles decreased by increasing the fiber density of the nanospheres. Moreover, the DFNS samples synthesized with primary alcohols of longer carbon chains exhibited broad spectral features in their SAXS patterns, indicating a lower degree of structural ordering. In contrast, the samples synthesized with shorter-chain and branched alcohols and diols showed sharp peaks, suggesting more ordered mesostructures like SBA-15 and MCM-41. Finally, the thermal stability of all samples was confirmed by TGA with no significant weight loss up to 800 °C. Thus, in this study, we have shown that the fiber density, particle morphology, surface area, pore volume, and pore size of DFNS are strongly influenced by the length of the alcohol chain, branching, and number of hydroxyl groups. Although alcohol type and structure are the most important factors, changes in the alcohol/TEOS molar ratio also have an impact on the morphology, textural characteristics, and thermal behavior of DFNS, albeit to a smaller extent. These findings on the structural tuning of DFNS open paths for the design of tailored nanomaterials for applications such as catalysis, drug delivery, and environmental remediation, where control over the surface area and porosity is crucial.

Data availability

All authors confirm that the data supporting the findings of this study are available within the article and its ESI.†

Author contributions

Jawed Qaderi: conceptualization, data curation, formal analysis, investigation, methodology, validation, visualization, writing – original draft, writing – review & editing; Maryam Radjabian: conceptualization, project administration, supervision, writing – review & editing; Martin Held: investigation, writing – review & editing; Anke-Lisa Höhme: investigation, writing – review & editing; Erik Schneider: investigation, writing – review & editing; Joachim Koll: investigation, writing – review & editing; Sandra König: investigation, writing – review & editing; Andreas Meyer: investigation, writing – review & editing; Michael Fröba: writing – review & editing; Volker Abetz: conceptualization, funding acquisition, resources, supervision, writing – review & editing.

Conflicts of interest

There are no conflicts to declare.

Acknowledgements

The authors would like to express their deepest gratitude to the German Academic Exchange Service (DAAD) for providing Jawed Qaderi with a PhD scholarship in Physical Chemistry under the scheme of the Hilde Domin Program. We also thank Dr Evgeni Sperling for his expert assistance and insightful contributions to the SEM analysis. We would also like to express our gratitude to Dr Birgit Hankiewicz for her help with the DLS measurements and thank Silvio Neumann for conducting the TGA measurements. This work benefited from the use of the SasView application, originally developed under the NSF award DMR-0520547. SasView contains the code developed with funding from the European Union's Horizon 2020 research and innovation program under the SINE2020 project, grant agreement No. 654000. This open access publication was funded by the Helmholtz-Zentrum Hereon as part of the TIB-RSC-Platinum agreement with the Royal Society of Chemistry.

References

1 V. Polshettiwar, D. Cha, X. Zhang and J. M. Basset, *Angew Chem. Int. Ed. Engl.*, 2010, **49**, 9652–9656.
2 A. Maity, R. Belgamwar and V. Polshettiwar, *Nat. Protoc.*, 2019, **14**, 2177–2204.
3 A. Maity, A. Das, D. Sen, S. Mazumder and V. Polshettiwar, *Langmuir*, 2017, **33**, 13774–13782.
4 A. Maity and V. Polshettiwar, *ChemSusChem*, 2017, **10**, 3866–3913.
5 V. Polshettiwar, *Acc. Chem. Res.*, 2022, **55**, 1395–1410.
6 D. S. Moon and J. K. Lee, *Langmuir*, 2012, **28**, 12341–12347.
7 M. A. A. Aziz, A. A. Jalil, S. Triwahyono and S. M. Sidik, *Appl. Catal., A*, 2014, **486**, 115–122.
8 N. Bayal, B. Singh, R. Singh and V. Polshettiwar, *Sci. Rep.*, 2016, **6**, 24888.
9 R. Soltani, A. Marjani, M. Hosseini and S. Shirazian, *Chemosphere*, 2020, **239**, 124735.
10 H. E. Wogo, N. Silmi, D. P. Benu, F. V. Steky, K. M. Setiawan, S. Sudirman, M. W. Azzindani, R. R. Mukti and V. Suendo, *Langmuir*, 2025, **41**, 5794–5807.
11 B. Singh and V. Polshettiwar, *J. Mater. Chem. A*, 2016, **4**, 7005–7019.
12 C. Lv, L. Xu, M. Chen, Y. Cui, X. Wen, C.-e. Wu, B. Yang, F. Wang, Z. Miao, X. Hu and Q. Shou, *Fuel*, 2020, **278**, 118333.
13 T. J. Siang, A. A. Jalil, N. A. A. Fatah and M. E. Chung, *J. Environ. Chem. Eng.*, 2021, **9**, 104616.
14 Z. Dong, X. Le, C. Dong, W. Zhang, X. Li and J. Ma, *Appl. Catal., B*, 2015, **162**, 372–380.
15 N. F. Khusnun, A. A. Jalil, T. A. T. Abdullah, S. S. M. Latip, C. N. C. Hitam, A. A. Fauzi, N. S. Hassan, M. A. H. Aziz, A. F. A. Rahman, F. F. A. Aziz, M. Bahari, R. H. Adnan and R. Saravanan, *J. CO_2 Util.*, 2022, **58**, 101901.
16 S. M. Sadeghzadeh, *RSC Adv.*, 2016, **6**, 54236–54240.
17 A. Marjani and R. K. Mohammadi, *Sci. Rep.*, 2021, **11**, 10735.
18 G. Song, X. Guo, Q. Li, J. Liao, D. Wang, T. Yuan, L. Li, R. Fang, M. Zhang, Q. Shen, F. Zheng and J. Gong, *Food Control*, 2023, **152**, 109846.
19 H. Fan, B. Li, Z. Shi, L. Zhao, K. Wang and D. Qiu, *Ceram. Int.*, 2018, **44**, 2345–2350.
20 E. Febriyanti, V. Suendo, R. R. Mukti, A. Prasetyo, A. F. Arifin, M. A. Akbar, S. Triwahyono and I. N. Marsih, Ismunandar, *Langmuir*, 2016, **32**, 5802–5811.

21 J. Bahadur, A. Maity, D. Sen, A. Das and V. Polshettiwar, *Langmuir*, 2021, **37**, 6423–6434.
22 X. Li, X. Chen, G. Miao, H. Liu, C. Mao, G. Yuan, Q. Liang, X. Shen, C. Ning and X. Fu, *J. Mater. Chem. B*, 2014, **2**, 7045–7054.
23 D. Shen, J. Yang, X. Li, L. Zhou, R. Zhang, W. Li, L. Chen, R. Wang, F. Zhang and D. Zhao, *Nano Lett.*, 2014, **14**, 923–932.
24 M. Kalantari, Y. Liu, E. Strounina, Y. Yang, H. Song and C. Yu, *J. Mater. Chem. A*, 2018, **6**, 17579–17586.
25 X. Du, X. Li and J. He, *ACS Appl. Mater. Interfaces*, 2010, **2**, 2365–2372.
26 C. Xu, M. Yu, O. Noonan, J. Zhang, H. Song, H. Zhang, C. Lei, Y. Niu, X. Huang and Y. Yang, *Small*, 2015, **11**, 5949–5955.
27 A. Ahmad, N. D. Zakaria, Z. Lockman and K. F. A. Razak, *J. Phys.: Conf. Ser.*, 2018, 1082.
28 D. Niu, Z. Ma, Y. Li and J. Shi, *J. Am. Chem. Soc.*, 2010, **132**(43), 15144–15147.
29 M. Mirzaei, M. B. Zarch, M. Darroudi, K. Sayyadi, S. T. Keshavarz, J. Sayyadi, A. Fallah and H. H. Maleki, *Appl. Sci.*, 2020, **426**, 7533.
30 X. Wang, Y. Liu, H. Xu, M. Dai, P. Qiao, W. Wang, Y. Liu and H. Song, *Appl. Surf. Sci.*, 2022, **603**, 154414.
31 Y. Feng, A. Schaefer, A. Hellman, M. Di, H. Härelind, M. Bauer and P.-A. Carlsson, *Langmuir*, 2022, **38**, 12859–12870.
32 Y. Xia, X. Xia and H. C. Peng, *J. Am. Chem. Soc.*, 2015, **137 25**, 7947–7966.
33 S. Okeil, S. Rabet, G. Valadez Huerta, G. Raabe and G. Garnweitner, *Langmuir*, 2024, **40**, 19343–19356.
34 G. Palazzo, F. Lopez, M. Giustini, G. Colafemmina and A. Ceglie, *J. Phys. Chem. B*, 2003, **107**, 1924–1931.
35 S. Sharma, N. Pal, P. K. Chowdhury, S. Sen and A. K. Ganguli, *J. Am. Chem. Soc.*, 2012, **134**, 19677–19684.
36 A. J. Mills, J. Wilkie and M. M. Britton, *J. Phys. Chem. B*, 2014, **118**, 10767–10775.
37 N. A. A. Fatah, A. A. Jalil, M. L. Firmansyah, S. Triwahyono, H. D. Setiabudi and D. V. N. Vo, *Int. J. Hydrogen Energy*, 2021, **46**, 24676–24686.
38 D. Sen, A. Maity, J. Bahadur, A. Das and V. Polshettiwar, *Microporous Mesoporous Mater.*, 2021, **323**, 111234.
39 M. Y. Shahul Hamid, A. Abdul Jalil, A. F. Abdul Rahman and T. A. Tuan Abdullah, *React. Chem. Eng.*, 2019, **4**, 1126–1135.
40 S. Shirazian, N. Pirestani, A. E. G. Baker and R. Soltani, *npj Clean Water*, 2025, **8**, 3.
41 E. Febriyanti, N. Silmi, V. Suendo, R. R. Mukti, P. U. Vivitasari, D. R. Adhika and Y. Majima, Suprijadi and Ismunandar, *Langmuir*, 2022, **38**, 1368–1379.
42 N. V. Thampi, K. Ojha and U. G. Nair, *J. Surfactants Deterg.*, 2013, **17**, 371–381.
43 G. Guerin, F. Qi, G. Cambridge, I. Manners and M. A. Winnik, *J. Phys. Chem. B*, 2012, **116**, 4328–4337.
44 M. Wasilewska, Z. Adamczyk and B. Jachimska, *Langmuir*, 2009, **25**, 3698–3704.
45 B. Di Credico, E. Manzini, L. Viganò, C. Canevali, M. D'Arienzo, S. Mostoni, R. Nisticò and R. Scotti, *Ceram. Int.*, 2023, **49**, 26165–26181.
46 H. S. Vaziri, I. A. Omaraei, M. Abadyan, M. Mortezaei and N. Yousefi, *Mater. Des.*, 2011, **32**, 4537–4542.
47 J. Yang, C.-R. Han, J.-F. Duan, F. Xu and R.-C. Sun, *Nanoscale*, 2013, **5**, 10858–10863.
48 Z. Zhou, Q. Li and X. Zhao, *Langmuir*, 2006, **22**, 3692–3697.
49 A. Maskara and D. M. Smith, *J. Am. Ceram. Soc.*, 1997, **80**, 1715–1722.
50 K. S. Sing, *Pure Appl. Chem.*, 1985, **57**, 603–619.
51 K. S. Sing and R. T. Williams, *Adsorpt. Sci. Technol.*, 2004, **22**, 773–782.
52 K. A. Cychosz and M. Thommes, *Engineering*, 2018, **4**, 559–566.
53 K. Palanichamy, S. Umasankar, S. Ganesh and N. Sasirekha, *Int. J. Hydrogen Energy*, 2023, **48**, 11727–11745.
54 A. A. Abdulrasheed, A. A. Jalil, M. Y. S. Hamid, T. J. Siang and T. A. T. Abdullah, *J. CO_2 Util.*, 2020, **37**, 230–239.
55 S. M. Yusof, R. Othaman, H. D. Setiabudi and L. P. Teh, *J. Solid State Chem.*, 2021, **294**, 121845.
56 M. Y. S. Hamid, M. L. Firmansyah, S. Triwahyono, A. A. Jalil, R. R. Mukti, E. Febriyanti, V. Suendo, H. D. Setiabudi, M. Mohamed and W. Nabgan, *Appl. Catal., A*, 2017, **532**, 86–94.
57 L. L. Hussami, R. W. Corkery and L. Kloo, *Carbon*, 2010, **48**, 3121–3130.
58 S. Reiser and M. Türk, *J. Supercrit. Fluids*, 2019, **144**, 122–133.
59 R. Janus, M. Wądrzyk, M. Lewandowski, P. Natkański, P. Łątka and P. Kuśtrowski, *J. Ind. Eng. Chem.*, 2020, **92**, 131–144.
60 E. Ramírez-Meneses, K. Philippot, M. A. Domínguez-Crespo, M. Ibrahim, I. Betancourt, A. M. Torres-Huerta and A. Ezeta-Mejia, *J. Mater. Sci.*, 2018, **53**, 8933–8950.
61 E. P. Barrett, L. G. Joyner and P. P. Halenda, *J. Am. Chem. Soc.*, 1951, **73**, 373–380.
62 Y. Liu, M. Paskevicius, M. V. Sofianos, G. Parkinson, S. Wang and C.-Z. Li, *Fuel*, 2021, **292**, 120384.
63 C. Schlumberger, C. Scherdel, M. Kriesten, P. Leicht, A. Keilbach, H. Ehmann, P. Kotnik, G. Reichenauer and M. Thommes, *Microporous Mesoporous Mater.*, 2022, **329**, 111554.
64 U. Patil, A. Fihri, A.-H. Emwas and V. Polshettiwar, *Chem. Sci.*, 2012, **3**, 2224–2229.
65 N. H. Nguyen, N.-H. Truong-Thi, D. T. D. Nguyen, Y. C. Ching, N. T. Huynh and D. H. Nguyen, *Colloids Surf., A*, 2022, **655**, 130218.
66 R. Kishor and A. K. Ghoshal, *Chem. Eng. J.*, 2015, **262**, 882–890.
67 H. S. Oboudatian and J. Safaei-Ghomi, *Res. Chem. Intermed.*, 2022, **48**, 2069–2085.
68 P. B. Sarawade, J.-K. Kim, A. Hilonga, D. V. Quang and H. T. Kim, *Microporous Mesoporous Mater.*, 2011, **139**, 138–147.
69 M. Fakhariha, A. A. Rafati, A. D. Garmakhany and A. Z. Asl, *Sci. Rep.*, 2025, **15**, 1–18.
70 M. Pishnamazi, H. Hafizi, M. Pishnamazi, A. Marjani, S. Shirazian and G. M. Walker, *Sci. Rep.*, 2021, **11**, 535.
71 V. Candela-Noguera, P. Amorós, E. Aznar, M. D. Marcos and R. Martínez-Máñez, *Microporous Mesoporous Mater.*, 2024, **373**, 113119.

